www.czasopisma.pan.pl PAN POLSKA AKADEMIA NAUK www.journals.pan.pl

PAN ARCHIVES OF ACOUSTICS
Vol. **43**, No. 3, pp. 455–463 (2018)

DOI: 10.24425/123917

The Acoustic Field Distribution Inside the Ultrasonic Ring Array

Wiktor STASZEWSKI, Tadeusz GUDRA, Krzysztof J. OPIELINSKI

Department of Acoustics and Multimedia
Faculty of Electronics
Wroclaw University of Science and Technology
Wybrzeze Wyspianskiego 27, 50-370 Wroclaw, Poland
e-mail: {wiktor.staszewski, tadeusz.gudra, krzysztof.opielinski}@pwr.edu.pl

(*received May 16, 2018; accepted June 20, 2018*)

This paper presents and analyses the results of a simulation of the acoustic field distribution in sectors of a 1024-element ring array, intended for the diagnosis of female breast tissue with the use of ultrasonic tomography. The array was tested for the possibility to equip an ultrasonic tomograph with an additional modality - conventional ultrasonic imaging with the use of individual fragments (sections) of the ring array. To determine the acoustic field for sectors of the ring array with a varying number of activated ultrasonic transducers, a combined sum of all acoustic fields created by each elementary transducer was calculated. By the use of MATLAB software, a unique algorithm was developed, for a numerical determination of the distribution of pressure of an ultrasonic wave on any surface or area of the medium generated by the concave curvilinear structure of rectangular ultrasound transducers with a geometric focus of the beam.

The analysis of the obtained results of the acoustic field distribution inside the ultrasonic ring array used in tomography allows to conclude that the optimal number of transducers in a sector enabling to obtain ultrasound images using linear echographic scanning is $32 \leq n \leq 128$, taking into account that due to an increased temporal resolution of ultrasonic imaging, this number should be as low as possible.

Keywords: ultrasound transmission tomography; acoustic field; ultrasonic multi-element array.

1. Introduction

There are currently several research centres around the world (Birk *et al.*, 2016; Duric *et al.*, 2007a; 2007b; Jirik *et al.*, 2012; Marmarelis *et al.*, 2007; Opieliński *et al.*, 2015; 2016; Wiskin *et al.*, 2013) that develop prototypes of ultrasonic tomographs for non-invasive and safe *in vivo* imaging of the female breast. Ultrasonic tomography imaging enables early detection of neoplastic lesions of breast tissue. The prototype of a multi-modal ultrasound computerized tomograph, implemented in Poland by a private investor in participation of a group of scientists from Wrocław University of Science and Technology (Opieliński *et al.*, 2015; 2016; 2018) uses a specialist ultrasonic ring array composed of many elementary piezoceramic transducers with a rectangular surface, evenly distributed on the inner side of the ring that surrounds the diagnosed breast submerged in water. The ultrasonic tomograph scans the whole breast using ultrasonic waves with a frequency of approx. 2 MHz from multiple angles and on many levels. It then processes the data and reconstructs images of individual coronal cross-sections in layers measuring a few millimetres. This device enables the reconstruction of two or three dimensional ultrasonic images of any cross-sections of the structure of the whole breast in three mutually complementary configurations (ultrasound modalities): ultrasound transmission tomography of acoustic velocity distribution (UTT_c), ultrasound transmission tomography of acoustic attenuation distribution (UTT_α), ultrasound reflection tomography (URT) (Opieliński *et al.*, 2018). Ongoing work is being carried out to equip the ultrasonic tomograph in an additional fourth modality, that is conventional ultrasonic imaging using individual fragments of sections of the ring array (Fig. 1a). This way, for each coronal cross-section of the breast it will be possible to obtain a 2D image constructed of multiple conventional ultrasonic images obtained automatically around the breast (Fig. 1b). In each multi-element section of transducers contained in the ring array it is pos-

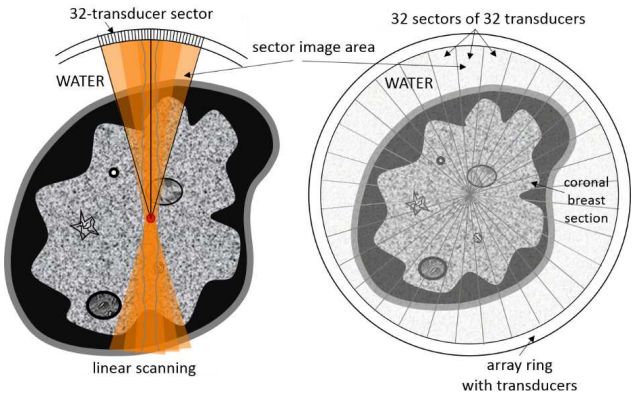

Fig. 1. The linear echographic scanning of the breast *in vivo* using fragments (sections of multiple transducers) of the ring array, with natural focusing on the axis of the transducer ring: a) the method of obtaining an image from a single section, b) diagram showing the combination of the cross-section of the breast from all sections.

sible to apply the same scanning method as in a linear ultrasonic array (Fig. 1a). The curvature of the ring array allows for a natural, geometrical focusing inside it.

A different method for scanning in each section may be phase-based scanning or a combination of phase-based and linear scanning known as *Compound Imaging* (CI) (Entrekin *et al.*, 1999; Opieliński *et al.*, 2014). These two scanning methods allow for obtaining images from individual sections with a divergent shape to the distance (inverted triangle in relation to linear scanning). Their circular structure and overlay eliminates image noise and interference that occurs as a result of blending common pixel areas. In each of the three scanning methods it is possible to optimise the location of the focus or implement multiple foci during the generation of an ultrasonic beam. It is important to use an appropriate, identical number of transducers in each section of the ring array in order to achieve a compromise between image quality and speed (temporal resolution). This paper presents such an attempt of optimisation through the analysis of the results obtained from calculations of the acoustic field for a linear scanning method in the section of the ring array with a different number of ultrasonic transducers.

2. Construction of the ring array

The ring array used in ultrasonic tomography is composed of 1024 elementary ultrasonic transducers that operate at a frequency of approx. 2 MHz (Opieliński *et al.*, 2015; 2018). The transducers are in the shape of rectangular tiles measuring 0.5×18 mm and are approx. 1 mm thick. They are evenly distributed with intervals of 0.3 mm on the inner side of the ring with a radius of $R_p = 130$ mm. Each elementary transducer can function as both a transmitter and a receiver. One of the ultrasonic ring arrays developed by the DARMIŃSKI S.A. company is shown in Fig. 2. Figure 3 shows the geometry of the array in the Cartesian coordinate system.

a)

b)

Fig. 2. One of the ultrasonic ring arrays developed by the DARMIŃSKI S.A. company: a) ring with ultrasonic transducers, b) a magnified image of a transducer fragment surface.

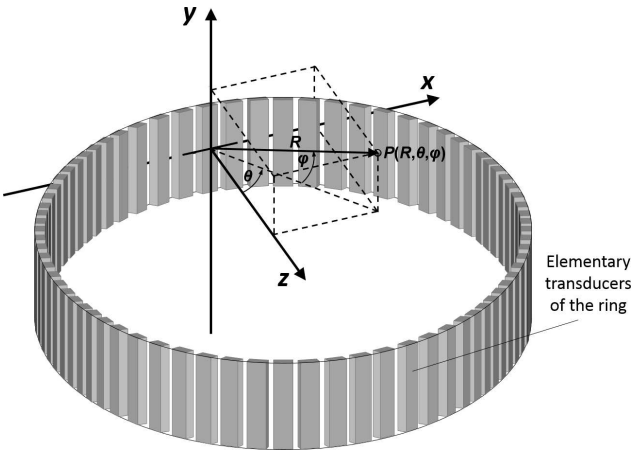

Fig. 3. The geometry of the array in the Cartesian coordinate system.

3. Calculation method

For the purpose of measuring the acoustic field created by transducers, the array was submerged in dis-

tilled water with a temperature of 25°C. The ring array is adapted to work in water. Water acts as a medium connecting the elementary transducers of the array and the biological medium, that is breast tissue diagnosed *in vivo*. The amplitude of acoustic velocity was estimated on the basis of measurements of acoustic pressure created in the water by the ultrasonic transducers of the ring array. Figure 4 shows an example of the shape of an ultrasonic wave impulse, registered in the water by a needle hydrophone from a distance of 5 mm from the surface of one of the ring array elementary transducers, on its axis, while stimulating the transducer with rectangular pulses with the length of 3 cycles, resonance frequency of $f_r = 2$ MHz and an amplitude of approx. 60 V_{pp}. The measured value of maximal voltage peak amplitude on the hydrophone terminal was approx. 150 mV_{pp}, which corresponds to the average peak value of acoustic pressure approx. $p = 430$ kPa.

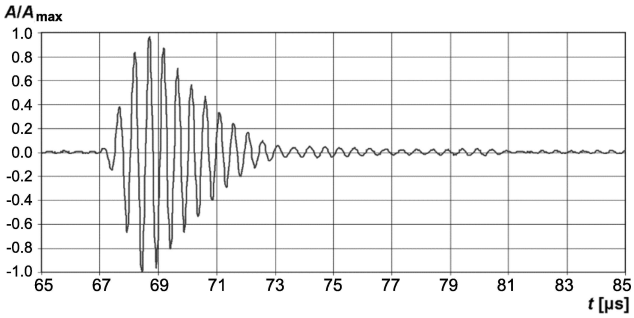

Fig. 4. Shape of an ultrasonic wave impulse registered in the water by a needle hydrophone from a distance of 5 mm from the surface of one of the elementary transducers of the ring array.

The acoustic velocity amplitude was calculated using the following equation:

$$V_o = \frac{p}{\rho_w c_w} = 0.288 \text{ m/s}, \tag{1}$$

where $\rho_w = 997.075$ kg/m^3 stands for the density of distilled water with a temperature of 25°C, and $c_w = 1496.728$ m/s stands for the ultrasonic wave propagation velocity in distilled water with a temperature of 25°C (Duck, 1990; Opieliński, 2011). The leaning amplitude of the pulsating water particle A_o corresponding to acoustic velocity V_o can be calculated using the following formula:

$$A_o = \frac{V_o}{\omega_r} = \frac{V_o}{2\pi f_r} = 23 \text{ nm}. \tag{2}$$

For the sector of the multi-element array, in which the elementary transducers are distributed on the inner side of the ring, a unique algorithm was developed using the MATLAB software, for a numerical determination of the distribution of pressure of an ultrasonic wave at the points $P(R, \theta, \varphi)$ on any surface of the medium in the far field, generated by the concave curvilinear structure of rectangular ultrasonic transducers as a sum of geometric transformations of fields calculated for all the elementary transducers of the sector (Fig. 5). For this purpose the following algorithm was applied (Opieliński, 2011):

$$p = \left| \sum_{i=0}^{n-1} -\frac{j\rho c k V_a}{2\pi R_i} ab \, e^{j(\omega t - kR_i)} \cdot \left[\frac{\sin\left(\frac{u_i a}{2}\right)}{\frac{u_i a}{2}} \right] \left[\frac{\sin\left(\frac{wb}{2}\right)}{\frac{wb}{2}} \right] \right|, \tag{3}$$

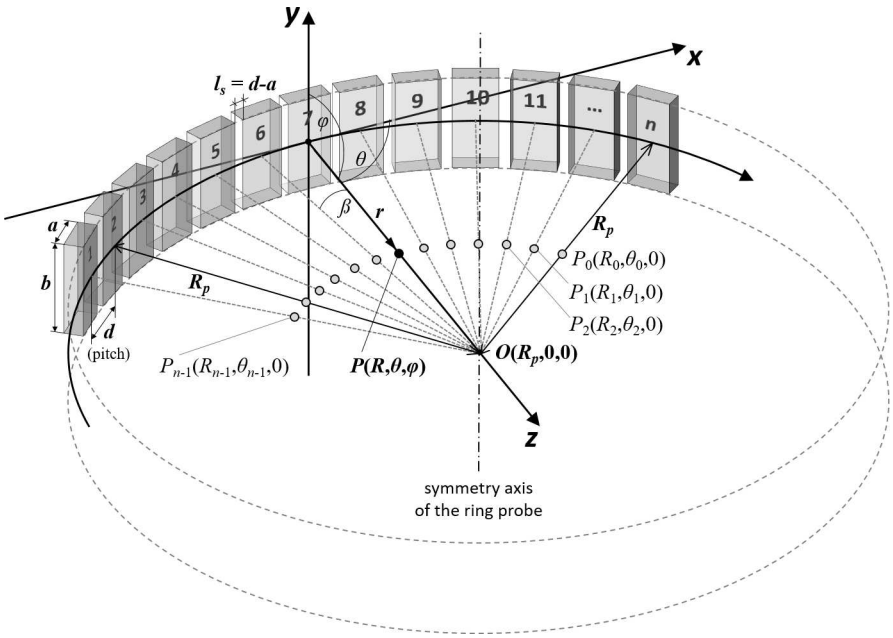

Fig. 5. Geometry of the ultrasonic ring array sector showing the sum of acoustic fields of the sector transducers.

where ρ – density of the medium, c – ultrasonic wave propagation velocity in the medium, $k = 2\pi/\lambda$ – wavenumber, $\lambda = c/f$ – wavelength, f – ultrasound frequency, $\omega = 2\pi f$ – cycle frequency of pulsations, t – time, V_a – acoustic velocity, a – width of the fundamental rectangular transducer, b – length of the fundamental rectangular transducer, $u_i = 2\pi \cdot \sin(\theta_i)/\lambda$, $w = 2\pi \cdot \sin(\phi)/\lambda$, R_i, θ_i, φ – polar coordinates of the point $P(R, \theta, \varphi)$, corrected in respect of the location $(i+1)$-th transducer in sector (see formula (4) and Fig. 5).

The far field in the horizontal plane of the rectangular elementary transducer with a width of $a = 0.5$ mm and resonance frequency of $f_r = 2$ MHz is $l_o = 0.35a^2/\lambda \approx 0.12$ mm.

The geometrical transformation of location of every point of the field $P(R, \theta, \varphi)$ in Eq. (3) is carried out symmetrically for every i+1th transducer in the sector (Fig. 5) by turning the point around the symmetry axis of the array with coordinates $O(r = R_p, \theta = 0)$ parallel to the axis Y (where R_p denotes the array's internal radius) by an appropriate multiplicity of the half of the angle $\beta = i \cdot 2\pi/N$ (where N is the number of all the transducers in the ring array). Corrected this way, the complex values of the pressure are then summed for all the n points, giving us the resultant pressure in each discussed point of the field $P(R, \theta, \varphi)$, generated by the analysed sector of the array. For the value of the pressure level at the point $P(R, \theta, \varphi)$ the influence of attenuation in the medium can also be taken into account. The corrected coordinates of the point $P(R, \theta, \varphi)$ for consecutive turns in the Cartesian coordinates (occurring in Eq. (3)) can be indicated by means of the following equations (Opieliński, 2011):

$$\begin{cases} r_i = \sqrt{r^2 + 4R_p^2 \sin^2 \frac{\beta_i}{2} + 2rR_p \cos(\theta - \beta_i) - 2R_p \cos\theta}, \\ \theta_i = \operatorname{arctg}\left(\dfrac{r\sin(\theta - \beta_i) + R_p \sin(\beta_i)}{r\cos(\theta - \beta_i) + 2R_p \sin^2 \frac{\beta_i}{2}} \right), \end{cases} \tag{4}$$

where, because of the necessity to maintain symmetry to the assumed setup of coordinates, $\beta_i = \left(\frac{n-1}{2} - i\right)\beta$ for the variability range $i = 0, ..., n-1$, where $i+1$ denotes the transducer number according to Fig. 5 and n is the number of transducers in the sector. In this paper, it is assumed that all transducers are identical and have an identical effectiveness and that their activation takes place at the same time ($t = 0$). Nevertheless, variation of the effectiveness of individual transducers of the array is possible in the presented calculation model by diversifying the proportional acoustic velocity values $V_a(i)$. This model also allows for dynamic focusing and a change in the direction of the ultrasonic wave beam by implementing adequate delays t_i in the factor $e^{j(\omega t_i - kR_i)}$ of formula (3).

4. Results

With the goal of analysing the acoustic field distribution for linear echographic scanning in concave curvilinear sections of the ring array, with a varying number of ultrasonic transducers, the level of acoustic pressure value was calculated using the following formula:

$$L_p = 20 \log\left(\frac{p(x, 0, z)}{p_o} \right), \tag{5}$$

with the reference pressure value applied in hydroacoustics $p_o = 1$ μPa. The acoustic pressure $p(x, 0, z)$ in a horizontal plane, half way up the length of the transducers (angle $\varphi = 0$) was determined in formulas (3) and (4). Attenuation in water was not taken into account in the calculations. The calculations were made in range x from −130 mm to 130 mm and z from 0 mm to 260 mm, setting of the array in the Cartesian coordinate system as shown in Fig. 3. Since an even number n of transducers in a section is taken into account during calculations, in order to maintain symmetry, the XYZ coordinate system has been tilted in the horizontal plane, allowing to set the centre of the system in axis of symmetry of the transducers. The set range of values x and z enables the visualisation of the acoustic field distribution on the whole interior of the ring array with a radius of $R_p = 130$ mm.

Figure 6 shows the results of calculating the acoustic field distribution $L_p(x, 0, z)$ for sectors of the ring array characterised by a varying number of activated transducers ($n = 4, 8, 16, 32, 64, 128, 256, 512$), in the form of pseudo-three-dimensional graphs. It was assumed that the number of transducers is always to the power of 2, due to the constructions of digitally driven systems of the array.

Figure 7 shows the results of the acoustic field distribution calculations in the form of $L_p(x, 0, z)$ for sectors of the ring array with varying numbers of activated transducers ($n = 4, 8, 16, 32, 64, 128, 256, 512$), in the form of black-and-white graphs.

Figure 8 shows the results of the acoustic field distribution calculations $L_p(x)$ for $y = 0$, on diameter of the ring array ($z = R_p = 130$ mm), for sectors of the ring array with varying numbers of activated transducers ($n = 4, 8, 16, 32, 64, 128, 256, 512$), in the form of linear distribution graphs (compare with Fig. 7 and Fig. 8).

The analysis of the obtained results shows that the focusing of the ultrasonic wave resulting from the curvature of the sector from a distance of $z = 130$ mm from its centre, begins to be clearly visible only for the number of transducers of the sector $n \geq 32$ (see Fig. 6 and Fig. 7). The level of acoustic pressure L_p in the focus increases logarithmically with the number of transducers (Fig. 8), which has been shown in Fig. 9.

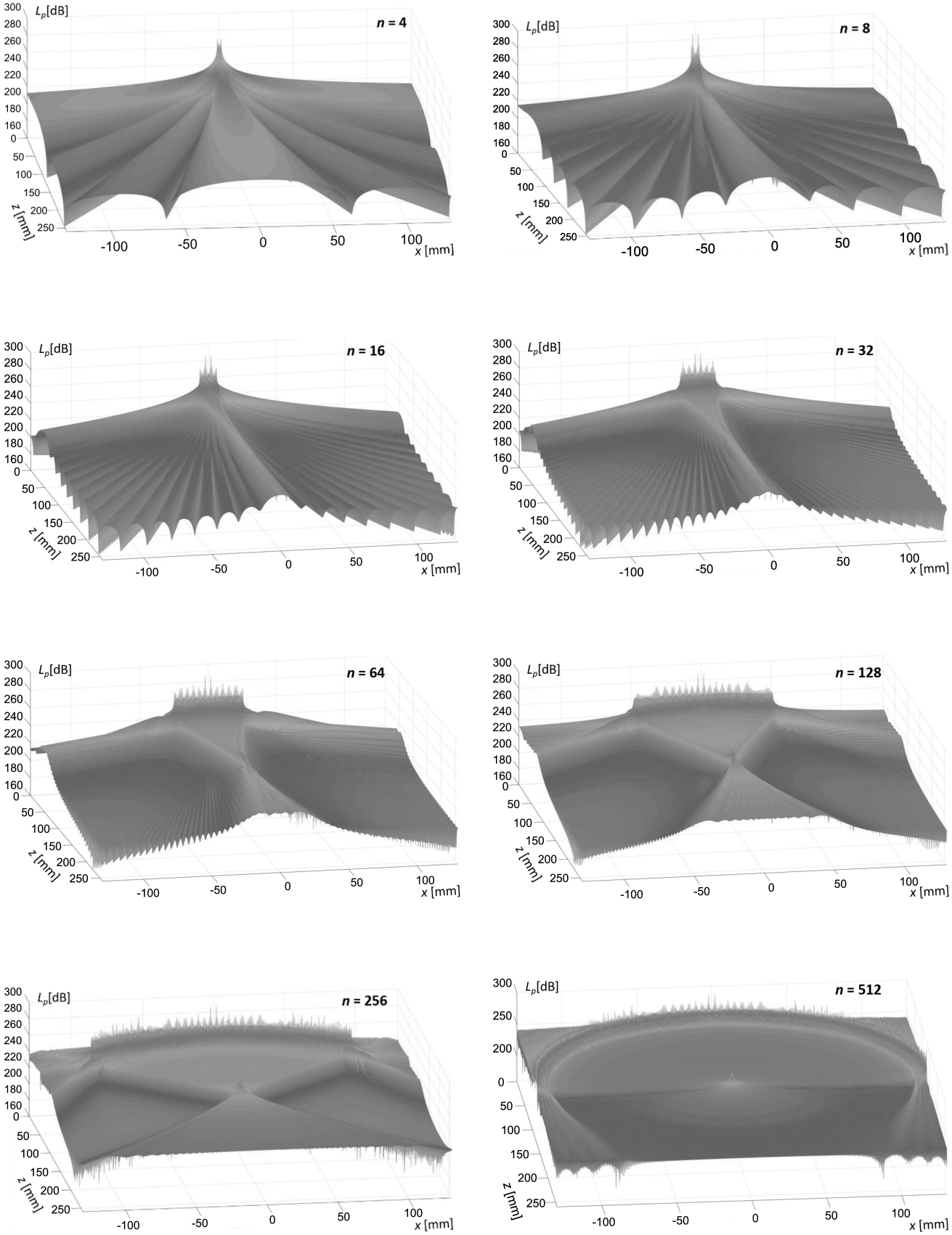

Fig. 6. The results of the acoustic field distribution calculations in the form of $L_p(x, 0, z)$ for sectors of the ring array with varying numbers of activated transducers (n = 4, 8, 16, 32, 64, 128, 256, 512), in the form of pseudo-three-dimensional graphs.

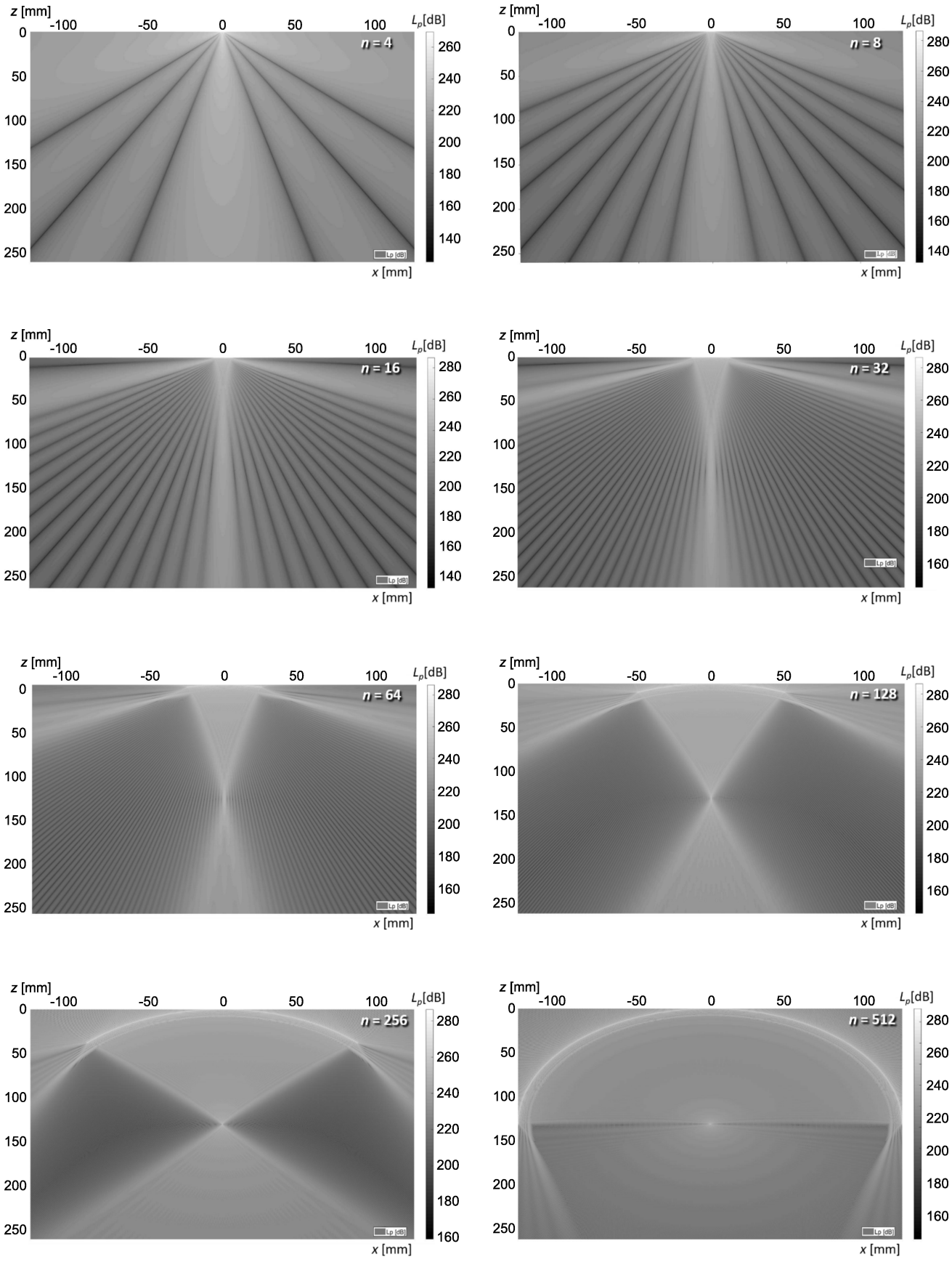

Fig. 7. Results of the acoustic field distribution calculations in the form of $L_p(x, 0, z)$ for sectors of the ring array with varying numbers of activated transducers ($n = 4$, 8, 16, 32, 64, 128, 256, 512), in the form of black-and-white graphs.

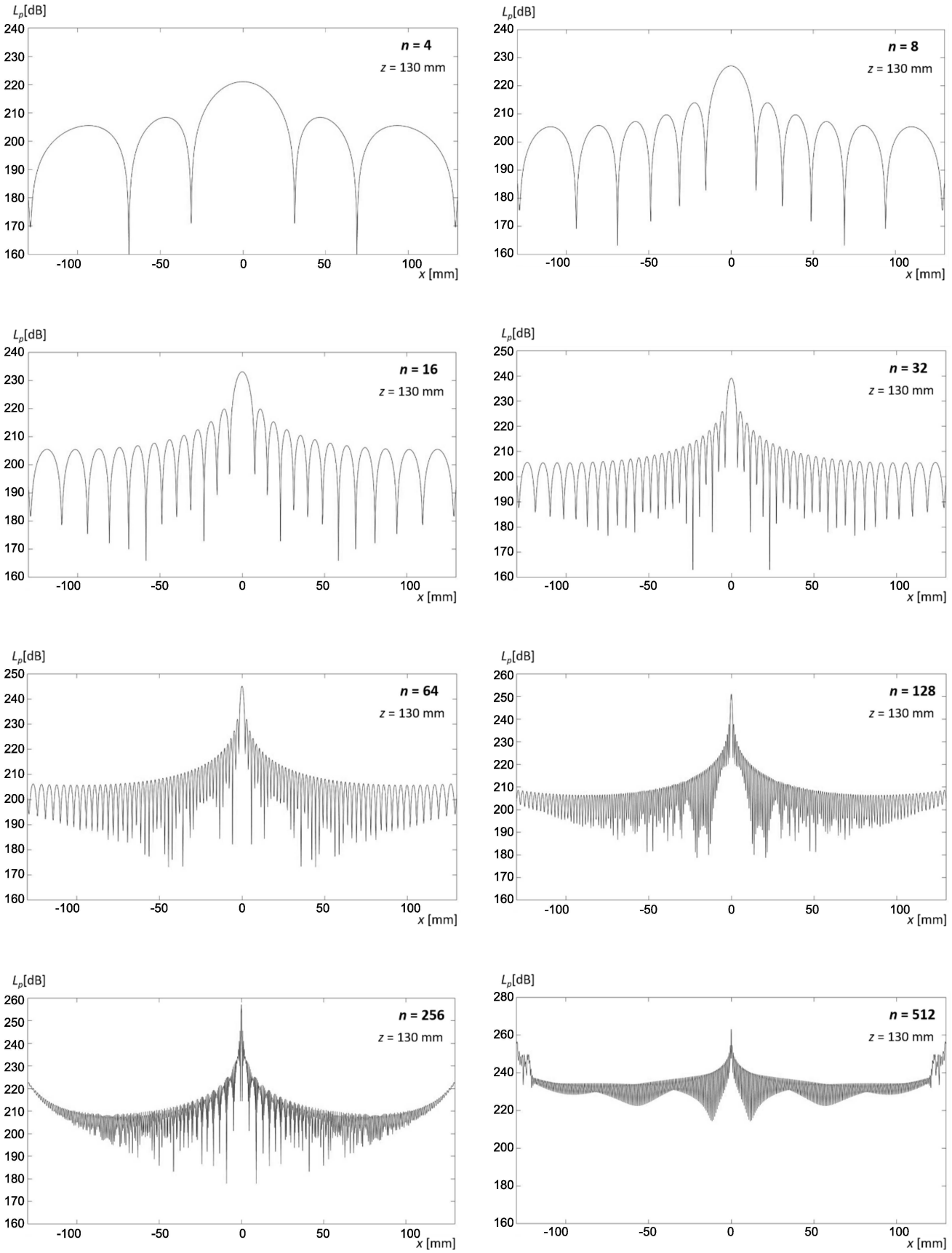

Fig. 8. Results of the acoustic field distribution calculations $L_p(x)$ for $y = 0$, on diameter of the ring array ($z = R_p =$ 130 mm), for sectors of the ring array with varying numbers of activated transducers ($n = 4$, 8, 16, 32, 64, 128, 256, 512), in the form of linear distribution graphs.

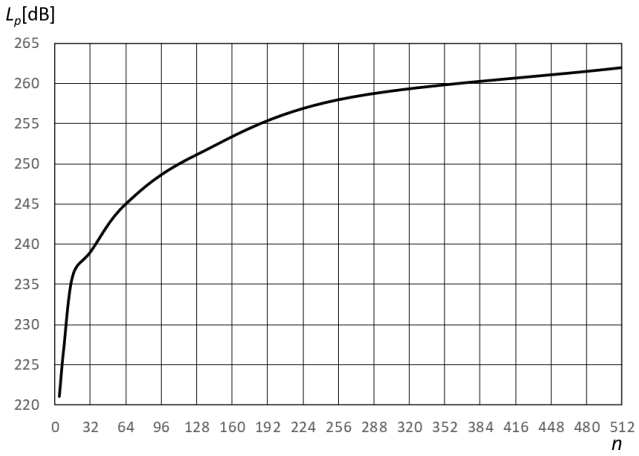

Fig. 9. The level of acoustic pressure in the focus of the array sector with relevance to its length.

The flattening and relative uniformity of the acoustic field without an increase in the level of acoustic pressure on both ends of the array diameter indicate sectors with the number of transducers $n \leq 128$.

With the goal of comparing the acoustic field distribution of individual sectors of the ring and linear arrays, Figs. 10–12 the results of calculations of the acoustic field distribution for linear array sectors without focusing ($t = 0$) are shown with the number of transducers $n = 32$ and $n = 64$, respectively in the form of pseudo-three-dimensional graphs, black-and-white graphs and linear distribution graphs. Calculations were done using formulas (3) and (4), assuming a large radius $R_p = 1000$ m and using identical values of the remaining parameters as in the case with sectors of the ring array.

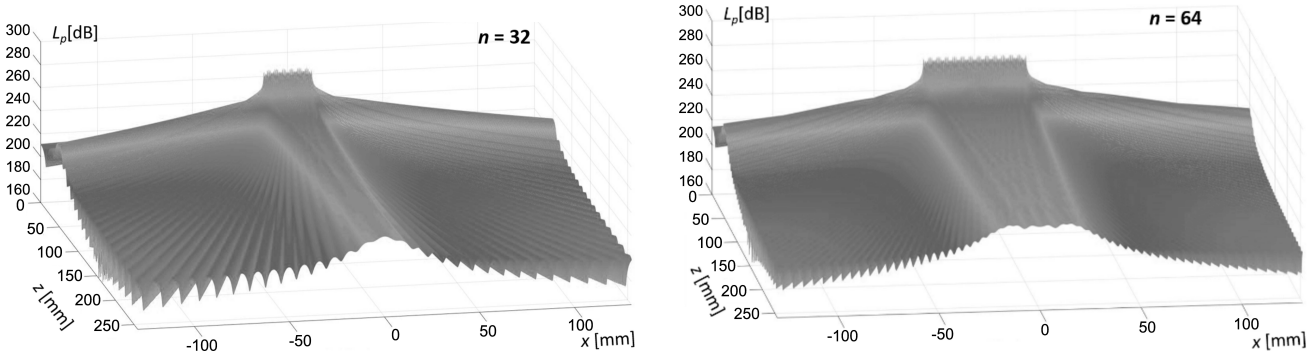

Fig. 10. Results of the acoustic field distribution $L_p(x, 0, z)$ for sectors of the linear array with the number of activated transducers $n = 32$ and $n = 64$, in the form of pseudo-three-dimensional graphs.

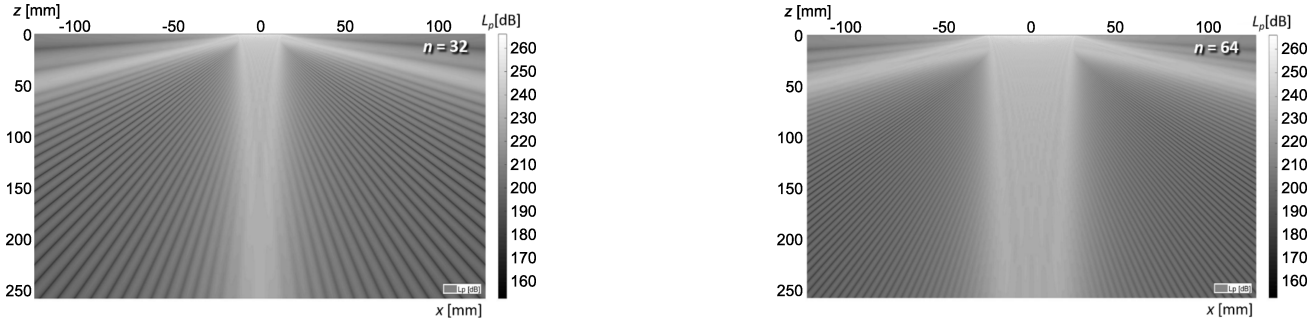

Fig. 11. Results of the acoustic field distribution $L_p(x, 0, z)$ for sectors of the linear array with the number of activated transducers $n = 32$ and $n = 64$, in the form of black-and-white graphs.

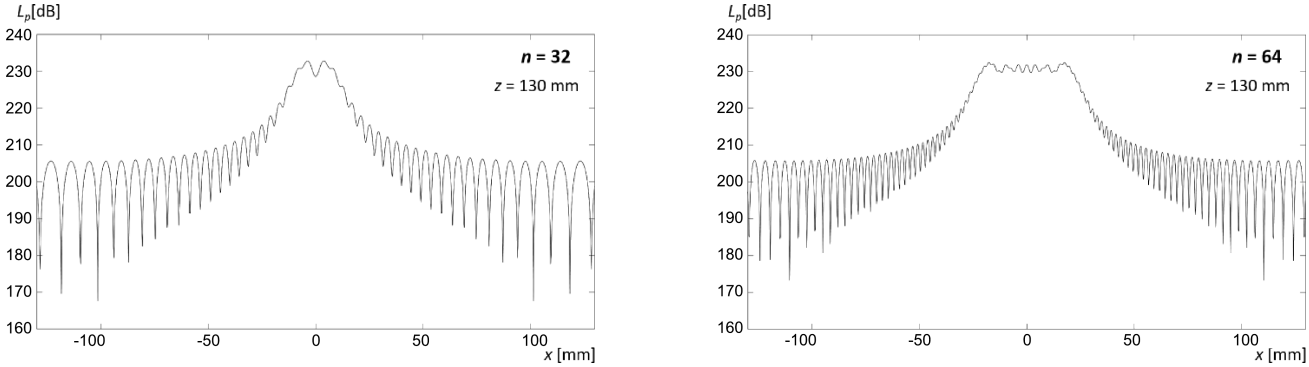

Fig. 12. Results of the acoustic field distribution $L_p(x)$ for $y = 0$, $z = 130$ mm, for sectors with the number of activated transducers $n = 32$ and $n = 64$, in the form of linear distribution graphs.

The acoustic field distributions of the linear array indicate the nature of a flat wave in the area of the sector with active transducers. For an increasing number of transducers, this area is more and more unified. For the number of transducers $n \geq 16$, the level of acoustic pressure distribution in this area does not change and is approx. 232 dB (Figs. 10–12).

5. Conclusions

The analysis of presented results of the calculations of the acoustic field distribution inside the ultrasonic ring array used in tomography allows to conclude that the optimal number of transducers in a sector that enable to obtain ultrasonic images using linear echographic scanning is $32 \leq n \leq 128$. The sectors with the number of transducers $n < 32$ show a very weak result of focusing inside the ring of the array, whereas sectors with the number of transducers $n > 128$ show a significant increase of the level of acoustic pressure on both ends the array diameter.

Together with the increase of activated transducers, the number of lateral lobes increases, whereas the main lobe is narrowed down. For the sector with the number of transducers $n = 32$, the width of the main lobe indicated by the decrease in acoustic pressure by 3 dB is approx. 5 mm, whereas, for the sector with the number of transducers $n = 64$ – the width is approx. 2 mm. Due to an increase in temporal resolution of ultrasonic imaging, which is defined as the amount of independent images registered in a unit of time (corresponding to the frequency of the image frame), a small number of activated transducers should be used in a sector.

The presented calculations shall be confirmed by further research by using ultrasonic imaging of cross-sections phantoms with the use of appropriate sectors of the ring array.

References

1. Birk M., Kretzek E., Figuli P., Weber M., Becker J., Ruiter N.V. (2016), *High-speed medical imaging in 3D ultrasound computer tomography*, IEEE Transactions on Parallel and Distributed Systems, **27**, 2, 455–467.
2. Duck F.A. (1990), *Physical properties of tissue. A comprehensive reference book*, 1st ed., Academic Press, London.
3. Duric N. *et al.* (2007), *Detection of breast cancer with ultrasound tomography: first results with the Computed Ultrasound Risk Evaluation (CURE) prototype*, Medical Physics, **34**, 2, 773–785.
4. Duric N., Littrup P., Schmidt S. *et al.* (2013), *Breast imaging with the SoftVue imaging system: first results*, [In:] *Medical Imaging 2013: Ultrasonic Imaging, Tomography, and Therapy*, Proceedings of SPIE, Bosch J.G., Doyley M.M. [Eds.], Vol. 8675, p. 86750K-1-8.
5. Entrekin R., Jackson P., Jago J.R., Porter B.A. (1999), *Real Time Spatial Compound Imaging in Breast Ultrasound: Technology and Early Clinical Experience*, Medica-Mundi, **43**, 3, 35–43.
6. Jirik R. *et al.* (2012), *Sound-speed image reconstruction insparse-aperture 3-D ultrasound transmission tomography*, IEEE Transactions on Ultrasonics, Ferroelectrics, and Frequency Control, **59**, 2, 254–264.
7. Marmarelis V.Z., Jeong J., Shin D.C., Do S. (2007), *High-resolution 3-D imaging and tissue differentiation with transmission tomography*, [in:] *Acoustical Imaging*, André M.P. *et al.* [Eds.], Vol. 28, Springer, Dordrecht, pp. 195–206.
8. Opieliński K.J. (2011), *Application of Transmission of Ultrasonic Waves for Characterization and Imaging of Biological Media Structures* [in Polish], Printing House of Wroclaw University of Science and Technology, Wroclaw.
9. Opieliński K.J. *et al.* (2015), *Imaging results of multi-modalultrasound computerized tomography system designed for breast diagnosis*, Computerized Medical Imaging and Graphics, **46**, 83–94.
10. Opieliński K.J. *et al.* (2016), *Breast ultrasound tomography: preliminary in vivo results*, [in:] *Information Technologies in Medicine*, Piętka E., Badura P., Kawa J., Wieclawek W. [Eds.], Vol. 1, Springer International Publishing, pp. 193–205.
11. Opieliński K.J. *et al.* (2018), *Multimodal ultrasound computer-assisted tomography: An approach to the recognition of breast lesion*, Computerized Medical Imaging and Graphics, **65**, 102–114.
12. Opielinski K.J., Pruchnicki P., Gudra T., Majewski J. (2014), *Full angle ultrasound spatial compound imaging*, [in:] Proceedings of 7th Forum Acusticum 2014 Joined with 61st Open Seminar on Acoustics and Polish Acoustical Society – Acoustical Society of Japan Special Session Stream [CD-ROM], Krakow: European Acoustics Association (ISSN 2221-3767).
13. Wiskin J. *et al.* (2013), *Three-dimensional nonlinear inverse scattering: quantitative transmission algorithms, refraction corrected reflection, scanner design and clinical results*, [in:] Proceedings of Meetings on Acoustics ICA2013, Vol. 19, No. 1, p. 075001, ASA.